

Gate-Tunable Topological Josephson Diode

Pei-Hao Fu^{1,2}, Yong Xu^{1,3}, Ching Hua Lee⁴, Yee Sin Ang^{2,*} and Jun-Feng Liu^{1†}

¹*School of Physics and Materials Science, Guangzhou University, Guangzhou 510006, China*

²*Science, Mathematics and Technology, Singapore University of Technology and Design (SUTD), 8 Somapah Road, Singapore 487372, Singapore*

³*Institute of Materials, Ningbo University of Technology, Ningbo 315016, China and*

⁴*Department of Physics, National University of Singapore, Singapore 117542*

Recent observation of superconducting diodes generalizes the category of the conventional electrical nonreciprocal phenomenon to the superconducting regime. The diode efficiency is commonly controlled by an external magnetic field which could, however, compromise the superconductivity of the system. In this work, we propose a concept of an all-electrical topological Josephson diode (TJD) in a time-reversal broken quantum spin Hall insulator hosting anisotropic helical edge states. Due to the edge states anisotropy and helicity, the electrostatic-induced Doppler energy shift results in a novel diode operation with a topologically protected maximal efficiency of 40% in a single edge setup which can be further boosted to 90% in a double-edge interferometer setup. Importantly, the diode operates in an all-electrical fashion, in which the efficiency and polarity can be efficiently modulated by an electrostatic gate voltage. The proposed gate-tunable TJD is within the current experimental reaches and shall offer useful building blocks for *topological superelectronics* that synergizes topological materials, superconductivity, and nonreciprocal quantum transport.

Introduction.- Recent observations of superconducting diodes (SCDs) in bulk superconductors [1–14] and Josephson junctions [15–29] generalizes conventional nonreciprocal phenomenon in electronics into the superconducting regime. The device concept of SCDs with dissipationless current flow in one direction while with a sizable resistance along the opposite is envisaged more than a decade ago [30]. The recent experimental realizations of SCDs have inspired a series of theoretical and computational works [31–54], suggesting a great wealth of exotic transport physics and device operations are yet to be unearthed in superconducting tunneling structures.

Generally, the efficiency of a diode is defined as

$$\eta = \frac{I_{c+} - I_{c-}}{I_{c+} + I_{c-}} \quad (1)$$

is used to quantify the diode, where $I_{c+/-}$ is the critical current along the positive/negative direction, and the sign of η defines the diode polarity. In most experiments, the modulation of the SCD efficiency and polarity is commonly achieved via the strength and direction of an external magnetic field. Such magnetic tuning knob, however, can destroy the superconductivity in the system and reintroduce significant dissipation to the system. Moreover, the experimentally reported diode efficiency is typically around 30% [see Fig. 1(d)], which may not be high enough for superconducting device technology [55]. An SCD with high efficiency, operation stability, and compatibility with non-magnetic modulation is in intense demand.

Topological Josephson diode (TJD) based on quantum spin Hall insulators (QSHIs) is a potential device architecture towards high-performance SCD [56–63],

whose diode behavior has been demonstrated [15, 42, 62–67]. For example, magnetic-flux-induced critical current asymmetry [42] has been observed [15, 62] in an inversion-symmetry broken QSHIs. In the presence of a finely tuned external magnetic field, the Doppler energy shift [64–67] causes directional-dependent critical current flows due to the anomalous Josephson effect [68–72] in a finite-momentum-Cooper-pair superconductor [51, 61, 73, 74], which offers another route towards efficient diode operation. However, magnetic field is still a necessary ingredient in TJDs.

Device concept of field-effect TJD.- In this work, we propose a TJD with all-electrical field-effect tunable diode efficiency by harnessing the unusual quantum transport behaviors of the anisotropic *tilted* helical edge states (AHESs) in a time-reversal-symmetry (TRS) broken QSHI [75–80][Fig. 1(a)]. Such Dirac bands tilting, together with the inherent spin-momentum locking of QSHI and an external *electrostatic field*, generate a peculiar gate-tunable Doppler energy shift in the superconducting leads [see Fig. 1(c) for a band diagram illustration] that facilitates the formation of finite-momentum Cooper pairs critical for the diode operation. Additionally, the tilted Dirac bands exhibit unequal quasiparticle group velocity between the forward and the backward propagations, which further boosts the directional-dependent current transport. The combination of Dirac band tilting, unequal quasiparticle group velocity, and gate-tunable Doppler energy shift provides an efficient mechanism to break the transport reciprocity, thus resulting in exceptional diode efficiency. Using scattering matrix formalism, analytical results for the current and diode efficiency are obtained in the short junction limit. A topologically protected maximal efficiency is expected to be 40% in a single edge at zero temperature. Remarkably, when considering a double junction, the diode efficiency of a double-current interferometer can be further

* yeesin'ang@sutd.edu.sg

† phjliu@gzhu.edu.cn

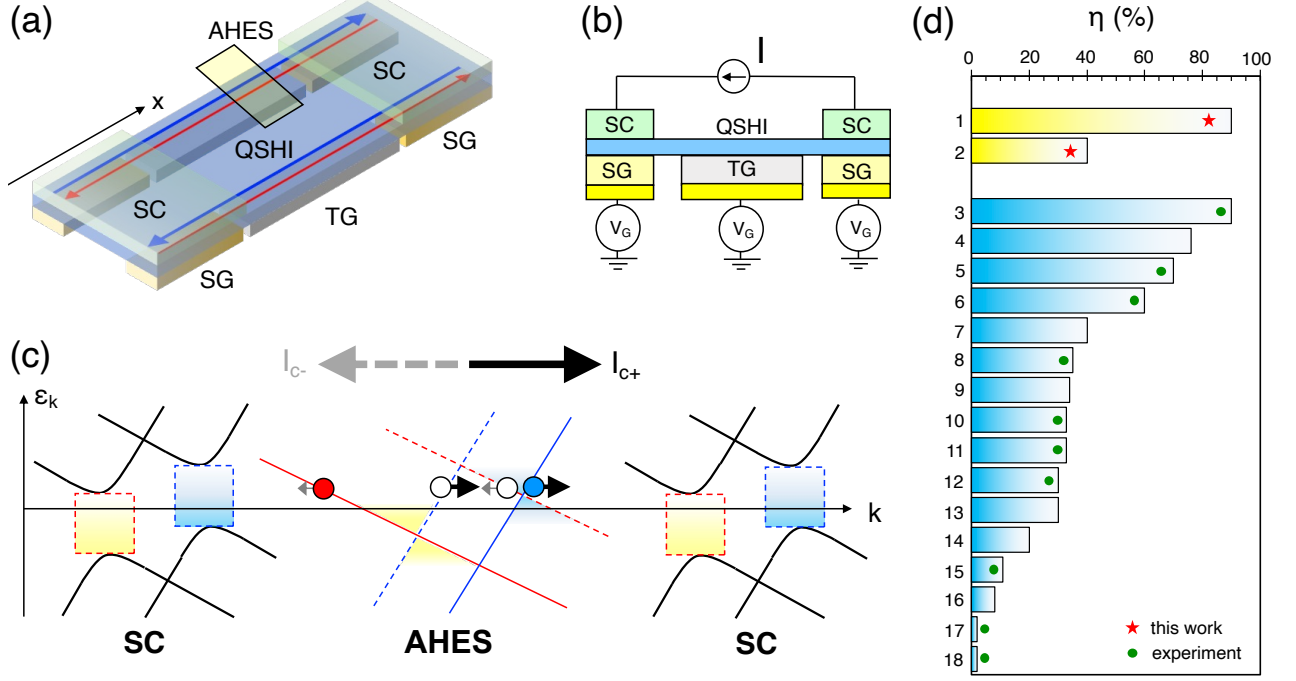


FIG. 1. (a) Schematic of a topological Josephson diode of quantum spin Hall insulator (QSHI) with by anisotropic helical edge states (AHESs), where the spin-up (spin-down) electrons propagate faster (slower) are labeled by thicker blue (thinner red) arrows. The superconducting (SC) leads and the central normal region are controlled by the super gates (SGs) and the tunneling gate (TG), respectively. (b) A side view of TJD. (c) Schematic of dispersions of the top edge states in the normal (central) and superconducting region (left and right). In the central region, the spin-up (spin-down) electron/hole band is represented by blue (red) solid/dashed line. (d) Diode efficiencies η for various systems labeled as 1. Single edge (this work), 2. double edge interferometer (this work), 3. Josephson triode [29], 4. supercurrent interferometers [52], 5. Nb with vortex [27], 6. high- T_c SC [28], 7. conventional SC with Meissner effect [51], 8. Pt/Y₃Fe₅O₁₂ [23], 9. chiral superconductor [26], 10. twisted bilayer graphene [16], 11. InAs [21, 22], 12. NiTe₂ [19], 13. Kekulé graphene [46], 14. surface states of 3D TI [54], 15. InAs [20], 16 and 17. InSb in Ref. [18] and Ref. [25] respectively, and 18. non-centrosymmetric SC [24].

boosted to an exceptionally high $\sim 90\%$ by locally tuning the electric potentials in each edge. The diode efficiency of the proposed TJD is among the highest reported in the literature thus far [see Fig. 1(d) for comparison with representative SCDs]. Importantly, gate-tunable current flow can be achieved in a long junction device, thus enabling the all-electrical modulation of the diode efficiency and polarity not commonly found in the vast majority of previously proposed TJDs. Importantly, the proposed device is within the current experimental reach. Since the Josephson junction is crucial for the TJD in this work is a potential building block towards *topological superelectronics* (i.e. superconductivity + electronics), which is helpful for quantum device technology, such as superconducting quantum interference devices and superconducting quantum computing bits, as well as cryogenic electronics that are critically needed for interface and control circuits to quantum computers [81].

Model.- To generate a nonreciprocal current, a Josephson junction carried by AHESs is constructed as shown in Fig. 1(a, b), whose Hamiltonian of the spin- σ mode

at the s edge is

$$H_{BdG}^{s,\sigma} = \int \Psi_{s,\sigma}^\dagger(x) \begin{pmatrix} h_e^{s,\sigma}(x) & \sigma\Delta(x) \\ \sigma\Delta^\dagger(x) & -[h_e^{s,\sigma}(-x)]^* \end{pmatrix} \Psi_{s,\sigma}(x) dx, \quad (2)$$

where the basis is $\Psi_{s,\sigma}(x) = [\psi_{s,\sigma}(x), \psi_{s,\bar{\sigma}}^\dagger(x)]^T$, and $h_e^{s,\sigma}(x) = s(\sigma\hbar v_0 + \hbar v_t)(-i\partial_x) - \mu^s(x)$ with $\mu^s(x) = \mu_{SC}^s\Theta(x^2 - dx) + \mu_N^s\Theta(dx - x^2)$ and $\Delta(x) = \Delta e^{i\varphi_L}\Theta(-x) + \Delta e^{i\varphi_R}\Theta(x - d)$. μ_{SC}^s (μ_N^s) is the chemical potential in the superconducting (normal) controlled by super (tunneling) gates. φ_L (φ_R) is the macroscopic phases of the left (right) SC lead and d is the length of the N region.

The dispersions of three regions are shown in Fig. 1(c). Particularly, in the SC region, there are two gaps above zero energy, $E_{g,\sigma} = \Delta_{\text{eff}}(1 + \sigma D^s)$, where $D^s = t\mu^s/\Delta_{\text{eff}}$ is a dimensionless variable representing a so-called Doppler energy shift [51, 64–67] in the unit of $\Delta_{\text{eff}} = \sqrt{1 - t^2}\Delta$, the effective superconducting gap modified by the anisotropy with strength $t = v_t/v_0 < 1$. More details are shown in the supplemental material [82]. Hereafter, we choose $\hbar v_0 = 1 = \Delta$ and $t = v_t/v_0 = 0.1$ as intrinsic parameters, so that D^s is solely determined by μ^s . Moreover, when $|D^s| > 1$, a gapless superconduct-

ing dispersion is possible because the proximity-induced superconductivity here does not have to obey the self-consistency equation [51].

The Doppler energy shift D^s is caused by a finite Cooper pair momentum $k_C^s = 2D^s\Delta/(\hbar v_0\sqrt{1-t^2})$ at each edge, which is crucial for realizing a Josephson diode [51, 64–66]. The dependency of D^s on μ^s allows a local control on the spatially separated edge supercurrents in experiments, resulting in an electrically optimized TJD.

A short-junction TJD.— To understand the effect of a finite Cooper pair momentum k_C^s or the Doppler energy shift D^s on the supercurrent, the Andreev bound state (ABS) is studied, which can be found by using the scattering matrix formalism [51, 82–84]. After calculations, the Andreev reflection (AR) amplitude for a spin- σ electron reflected as a spin- $\bar{\sigma}$ hole is

$$r_{A,\sigma} = \sigma e^{-i\theta_\sigma}, \quad (3)$$

with $\theta_\sigma = \cos^{-1}(E/\Delta_{\text{eff}} - \sigma D^t)$ for $|E/\Delta_{\text{eff}} - \sigma D^t| < 1$ and $\theta_\sigma = -i \cosh^{-1}(E/\Delta_{\text{eff}} - \sigma D^t)$ for $|E/\Delta_{\text{eff}} - \sigma D^t| > 1$. In the top edge, the AR coefficients $R_{A,\sigma} = |r_{A,\sigma}|^2$ with $D^t = 0.5$ in Fig. 2(a) exhibit a superconducting band gap shift due to Doppler energy shift, consistent with the dispersions schematized in Fig. 1(c). The spin-resolved AR coefficients keep units within the corresponding band gap and are antisymmetric to each other i.e. $R_{A,\sigma}(E) = R_{A,\bar{\sigma}}(-E)$. This leads to antisymmetric ABS spectra,

$$E_{s,\sigma} = \sigma \Delta_{\text{eff}} \left\{ s D^s - \cos\left(\frac{\varphi}{2}\right) \text{sign}\left[\sin\left(\frac{\varphi}{2}\right)\right] \right\}. \quad (4)$$

as depicted in Fig. 2(b), where two spin branches gain an opposite energy shift due to D^t and thus $E_{s,\sigma} = -E_{s,\bar{\sigma}}$. As a result, the topologically protected zero-energy crossing in ABS spectra is shifted from $\varphi = \pi$ to $\varphi = \varphi_c^s = 2 \cos^{-1}(s D^s)$ as labeled in Fig. 2(b). Additionally, for φ close to 0 and 2π , two spin branches gradually merge into the continuum states (not shown here) and the 2π -period spectra remain.

Usually, the sign of supercurrent inverts at the zero-energy crossing in ABS spectra, causing a sharp jump/raise from a positive/negative current to a negative/positive one, and the distinct behaviors of ABS spectra before and after φ_c^s result in an unequal current in the opposite direction.

The current-phase relation (CPR) in each edge can be determined by the corresponding free energy [51, 66, 83, 84]. Without parity constraint [57, 65, 66], at zero temperature, we have [82]

$$I_1^s(\varphi) = \frac{e\Delta_{\text{eff}}}{2\hbar} P(\varphi) \sin(\varphi/2) + \frac{e\Delta_{\text{eff}}}{2\hbar} s \frac{2}{\pi} D^s, \quad (5)$$

for $|D^s| < 1$, where the first and the second term on the right are the contributions from ABS and continuum states, respectively. In the former, $P(\varphi) = \text{sign}\{\cos(\varphi/2) - s D^s \text{sign}[\sin(\varphi/2)]\}$ is the ground-state parity of each edge. And the latter is phase-independent

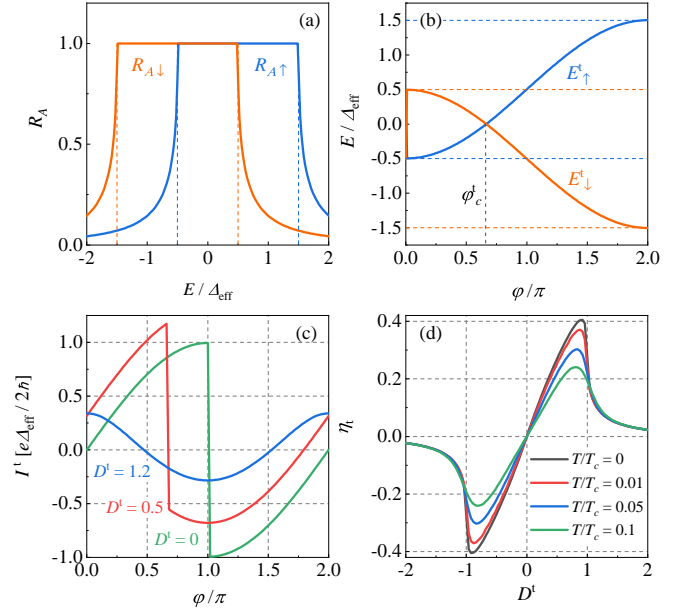


FIG. 2. (a) The energy dependence of Andreev reflection probabilities at N-SC interface of different spin channels. (b) The corresponding phase-dependent Andreev bound states. The topologically protected zero-energy crossing is shifted to $\varphi = \varphi_c^s = 2 \cos^{-1}(s D^s)$. (c) The current-phase relation of the TJD with different dimensionless Doppler energy shift D^t . (d) The dependence of diode efficiency via Doppler energy shift in different temperatures. We choose $\hbar v_0 = 1 = \Delta$ and $t = v_t/v_0 = 0.1$ and both the energy and the Doppler energy shift $D^s = t\mu_{SC}^t/\Delta_{\text{eff}}$ are normalized by the effective SC gap $\Delta_{\text{eff}} = \sqrt{1-t^2}\Delta$. In (a, b), and (d), we choose $D^s = 0.5$.

and directly induced by the Doppler energy shift. On the other hand, $|D^s| > 1$, we have

$$I_2^s(\varphi) = \text{sign}(s D^s) \frac{e\Delta_{\text{eff}}}{\pi\hbar} \Gamma(\varphi). \quad (6)$$

with $\Gamma(\varphi) = \frac{|D^s|}{\sqrt{(D^s)^2 - 1}} - \sin(\varphi/2) \tan^{-1}[\sin(\varphi/2)/\sqrt{(D^s)^2 - 1}]$.

The characteristics of CPR [Eq. (5)] shown in Fig. 2(c) are as follows. (i) The current jumps at $\varphi = \varphi_c^s$, corresponding to the topologically protected zero-energy crossing in ABS spectra. (ii) There is an anomalous Josephson current solely contributed by continuum states, i.e. $I_1^s(0) = I_{\text{cont}}^s$. And (iii), due to the continuum states, a TJD occurs with an efficiency ($|D^s| < 1$)

$$\eta_1^s = \text{sign}(s D^s) \frac{4|D^s|/\pi + \sqrt{1 - (D^s)^2} - 1}{\sqrt{1 - (D^s)^2} + 1}, \quad (7)$$

which vanishes as $D^s = 0$. On the other hand, when $|D^s| > 1$, the Josephson diode efficiency is

$$\eta_2^s = \text{sign}(s D^s) \frac{2(|D^s| - \sqrt{(D^s)^2 - 1}) - \cot^{-1} \sqrt{(D^s)^2 - 1}}{\cot^{-1} \sqrt{(D^s)^2 - 1}}, \quad (8)$$

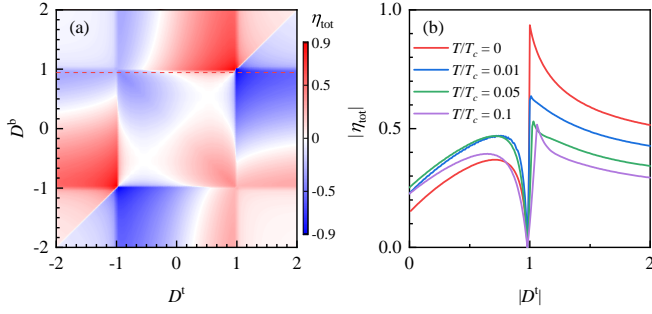


FIG. 3. (a) The density plot of the total diode efficiency of Doppler energy shift in the two edges, which shows an antisymmetry with respect to the line of $D^t = D^b$. (b) The absolute value of η_{tot} as a function of $|D^t|$ at different temperatures with $D^b = 0.95$. Other parameters are chosen as Fig. 2.

which also vanishes when $|D^s| \gg 1$, since there is no asymmetry in the CPR $\lim_{|D^s| \gg 1} I_2^s = s(e\Delta_{\text{eff}}/h) \cos \varphi / D^s$ as shown in Fig. 2(c).

Therefore, at zero temperature, the maximum TJD efficiency is up to $|\eta^s| \sim 40.5\%$ when $|D^s| = 4\pi/(4 + \pi^2) \sim 0.906$, which reduces with a growing temperature as shown in Fig. 2(d).

In a conventional JDE, the efficiency is suppressed by disorders and the normal reflection at the N-SC interface due to the Fermi surface mismatches, which probably destroys the zero-energy crossing in the ABS spectrum so as to smoothen the jumps in the CPR and thus reduces the current asymmetry [51]. However, based on the helicity of the edge states, the JDE proposed here is topologically protected due to the prohibition of backscattering.

TJD in a double-edges interferometer.- When considering a supercurrent interferometer formed by two edges, the diode efficiency can be greatly optimized when $D^t > 1$ as exhibited in Fig. 3. These phenomena can be understood through the CPRs [82]. When $D^t > 1$ and $D^b = 0$, because of the nearly cosinoidal behavior of the top-edge current [see Eq. (6)], the positive (negative) critical current of $I^{\text{tot}}(\varphi)$ occurs as $\varphi \sim \pi$, due to a destructive (constructive) interference between two currents, i.e. $I_{c+/c-}^{\text{tot}} \sim I_{c+}^b + (-)I_2^t(\pi)$ [$I_2^t(\pi) < 0$]. Thus, the resulting diode efficiency is $\eta^{\text{tot}} = I_2^t(\pi)/I_{c+}^b$, which is measurable even through the diode effects of edge current nearly vanishes.

Now, by combining the effect of the interferometer and Doppler energy shift by turning on D^b , the diode efficiency is highly optimized to $\eta^{\text{tot}} \sim 90\%$ when $|D^{b,t}| \sim 1$ as shown in Fig. 3(a) which is antisymmetric with respect to the line $D^t = D^b$ where the diode effect vanishes due to the cancellation of the Doppler energy shifts between two edges as in the cases of the magnetic field [64–66]. Generally, a fully polarized diode with $|\eta^{\text{tot}}| = 1$ is impossible. This is restricted by the fact that the free energy is a single-valued function in one period, which indicates that when the critical current in one direction

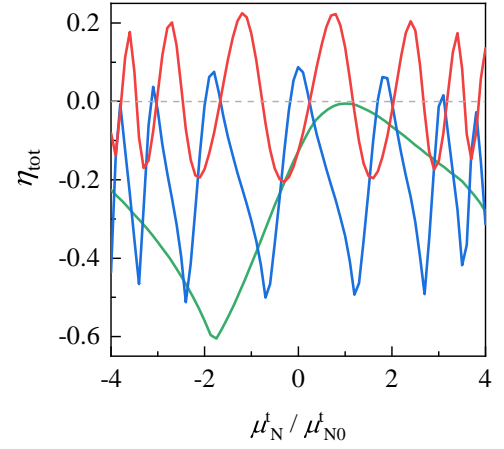


FIG. 4. Gate-tunable Josephson diode efficiency. We choose $D^b = 0$ ($D^b = 0.95$) for the red (blue) line. The length of the junction is $d = 80a$ ($a = 1$ is the lattice constant.). For the green line, we choose $d = 16a$ and $D^b = 0.95$. Other parameters are addressed in the supplement material [82].

is zero, its opposite-direction counterpart must vanish.

Such a high diode efficiency indicates that a nearly fully unidirectional supercurrent is the first result of this work. Although diode efficiency decreases as depicted in Fig. 3(b) as the temperature increases, it remains higher than the one in a single edge.

Gate-tunable field-effect topological Josephson diode.- The tunneling junction behaves as a three-terminal field-effect topological Josephson diode (FETJD), where the diode efficiency can be switched on and off while the diode polarity can be reversed by the gate voltage for a tunneling junction with a sizable length in the N region. To obtain the results of an arbitrary-length junction, we numerically simulate [82] a tight-binding model of QSHI using time-reversal broken Bernevig-Hughes-Zhang model [87–89]. The results can effectively describe the TJD transistor in a Floquet QSHI [76–78] or the states around the Γ point of few-layer antiferromagnetic MnBi_2Te_4 [79, 80].

By means of the lattice Green’s function technique [82, 90, 91], the CPR can be qualitatively described as $I^{\text{tot}} = \sum_s I^s(\varphi^s)$ with $\varphi^s = \varphi + \varphi_K^s + \varphi_g^s$, where $\varphi_K^s \sim s2k_F^s d$ is another additional phase accumulated by the finite-momentum Cooper pairs [51] and $\varphi_g^s = 2t\mu_N^s d[\hbar v_F(1 - t^2)]^{-1}$ is the gate-control phase from the electron-hole pairs accumulated in the N region [78].

As a result, a FETJD can be constructed based on the phase difference between the component currents in a QSHI interferometer can be manipulated by the gate voltage. As exhibited in Fig. 4, the polarity can be rapidly reversed when $D^b < 1$, and the efficiency can be switched on/off with a maximal up to 60% when $D^b > 1$. This device greatly enhances the flexibility in designing future superconducting circuits technology.

Discussions and conclusions.- Experimentally, FETJD is expected to be realized in superconducting magnetic

doped QSHIs [59, 88] and the recently investigated superconducting-proximity MnBi_2Te_4 family [92, 93]. The typical superconducting proximate gaps in QSHIs are in the order from 0.1 meV in HgTe [15, 61] and MnBi_2Te_4 [92, 93] to 1 meV in WTe_2 [62, 63], corresponding to the critical current in the order of tens of nanoamperes, which is detectable in the current experiments [17, 19, 21, 22]. Besides, the Fermi levels within each edge can be controlled by side gates or lateral gates as in the experiments involving Josephson field-effect transistor [94, 95]. Recently, we note that a gate-tunable JD is experimentally achieved in InSb nanowires [25], which may share a similar mechanism proposed in this work.

In conclusion, we proposed a mechanism to achieve gate-tunable field-effect topological Josephson diode using AHESs within a time-reversal-symmetry broken QSHI. An electrically manipulable TJD is generated by a Doppler energy shift, due to the anisotropy and helicity nature of the topological edge states. The topologically protected maximal diode efficiency is 40% in a single edge, which is immensely optimized to be nearly fully unidirectional with an efficiency reaching 90% in

a double-edge interferometer. Moreover, the diode efficiency can be switched on/off and its polarity can be reversed by controlling the gate voltage. Since the interplay of topological material, Josephson junction, and nonreciprocity plays a fundamental role in various applications such as topological superconducting calculations, we believe the theoretical proposals here have potential application in topologically superconducting electronics in the near future.

ACKNOWLEDGMENTS

P.-H. Fu thanks W. Xu, S.-H. Zheng, S. Li, and J. Li for inspiring discussions. P.-H. Fu & Y. S. Ang are supported by the Singapore Ministry of Education (MOE) Academic Research Fund (AcRF) Tier 2 Grant (MOE-T2EP50221-0019). J.-F. Liu is supported by the National Natural Science Foundation of China (Grants No. 12174077) and Natural Science Foundation of Guangdong Province (Grant No. 2021A1515012363).

-
- [1] R. Wakatsuki, Y. Saito, S. Hoshino, Y. M. Itahashi, T. Ideue, M. Ezawa, Y. Iwasa, and N. Nagaosa, Nonreciprocal Charge Transport in Noncentrosymmetric Superconductors, *Sci. Adv.* **3**, e1602390 (2017).
 - [2] E. Zhang, X. Xu, Y.-C. Zou, L. Ai, X. Dong, C. Huang, P. Leng, S. Liu, Y. Zhang, Z. Jia, X. Peng, M. Zhao, Y. Yang, Z. Li, H. Guo, S. J. Haigh, N. Nagaosa, J. Shen, and F. Xiu, Nonreciprocal Superconducting NbSe_2 Antenna, *Nat. Commun.* **11**, 5634 (2020).
 - [3] F. Ando, Y. Miyasaka, T. Li, J. Ishizuka, T. Arakawa, Y. Shiota, T. Moriyama, Y. Yanase, and T. Ono, Observation of Superconducting Diode Effect, *Nature* **584**, 373 (2020).
 - [4] T. Schumann, L. Galletti, H. Jeong, K. Ahadi, W. M. Strickland, S. Salmani-Rezaie, and S. Stemmer, Possible Signatures of Mixed-Parity Superconductivity in Doped Polar SrTiO_3 Films, *Phys. Rev. B* **101**, 100503 (2020).
 - [5] L. Bauriedl, C. Bäuml, L. Fuchs, C. Baumgartner, N. Paulik, J. M. Bauer, K.-Q. Lin, J. M. Lupton, T. Taniguchi, K. Watanabe, C. Strunk, and N. Paradiso, Supercurrent Diode Effect and Magnetochiral Anisotropy in Few-Layer NbSe_2 , *Nat. Commun.* **13**, 4266 (2022).
 - [6] Y. M. Itahashi, T. Ideue, Y. Saito, S. Shimizu, T. Ouchi, T. Nojima, and Y. Iwasa, Nonreciprocal Transport in Gate-Induced Polar Superconductor SrTiO_3 , *Sci. Adv.* **6**, eaay9120 (2020).
 - [7] J. Shin, S. Son, J. Yun, G. Park, K. Zhang, Y. J. Shin, J.-G. Park, and D. Kim, Magnetic Proximity-Induced Superconducting Diode Effect and Infinite Magnetoresistance in van Der Waals Heterostructure, *arXiv: 2111.05627* (2021).
 - [8] Y.-Y. Lyu, J. Jiang, Y.-L. Wang, Z.-L. Xiao, S. Dong, Q.-H. Chen, M. V. Milošević, H. Wang, R. Divan, J. E. Pearson, P. Wu, F. M. Peeters, and W.-K. Kwok, Superconducting Diode Effect via Conformal-Mapped Nanoholes, *Nat. Commun.* **12**, 2703 (2021).
 - [9] K. Yasuda, H. Yasuda, T. Liang, R. Yoshimi, A. Tsukazaki, K. S. Takahashi, N. Nagaosa, M. Kawasaki, and Y. Tokura, Nonreciprocal Charge Transport at Topological Insulator/Superconductor Interface, *Nat. Commun.* **10**, 2734 (2019).
 - [10] Y. Wu, Q. Wang, X. Zhou, J. Wang, P. Dong, J. He, Y. Ding, B. Teng, Y. Zhang, Y. Li, C. Zhao, H. Zhang, J. Liu, Y. Qi, K. Watanabe, T. Taniguchi, and J. Li, Nonreciprocal Charge Transport in Topological Kagome Superconductor CsV_3Sb_5 , *arXiv: 2210.10437* (2022).
 - [11] M. Masuko, M. Kawamura, R. Yoshimi, M. Hirayama, Y. Ikeda, R. Watanabe, J. J. He, D. Maryenko, A. Tsukazaki, K. S. Takahashi, M. Kawasaki, N. Nagaosa, and Y. Tokura, Nonreciprocal Charge Transport in Topological Superconductor Candidate $\text{Bi}_2\text{Te}_3/\text{PdTe}_2$ Heterostructure, *Npj Quantum Mater.* **7**, 104 (2022).
 - [12] J.-X. Lin, P. Siriviboon, H. D. Scammell, S. Liu, D. Rhodes, K. Watanabe, T. Taniguchi, J. Hone, M. S. Scheurer, and J. I. A. Li, Zero-Field Superconducting Diode Effect in Small-Twist-Angle Trilayer Graphene, *Nat. Phys.* **18**, 1221 (2022).
 - [13] H. Narita, J. Ishizuka, R. Kawarazaki, D. Kan, Y. Shiota, T. Moriyama, Y. Shimakawa, A. V. Ognev, A. S. Samardak, Y. Yanase, and T. Ono, Field-Free Superconducting Diode Effect in Noncentrosymmetric Superconductor/Ferromagnet Multilayers, *Nat. Nanotechnol.* **17**, 823 (2022).
 - [14] Y. Hou, F. Nichele, H. Chi, A. Lodesani, Y. Wu, M. F. Ritter, D. Z. Haxell, M. Davydova, S. Ilić, O. Glezakou-Elbert, A. Varambally, F. S. Bergeret, A. Kamra, L. Fu, P. A. Lee, and J. S. Moodera, Ubiquitous Superconducting Diode Effect in Superconductor Thin Films, *arXiv: 2205.09276* (2022).
 - [15] E. Bocquillon, R. S. Deacon, J. Wiedenmann, P. Leub-

- ner, T. M. Klapwijk, C. Brüne, K. Ishibashi, H. Bühhmann, and L. W. Molenkamp, Gapless Andreev Bound States in the Quantum Spin Hall Insulator HgTe, *Nat. Nanotechnol.* **12**, 137 (2017).
- [16] J. Diez-Merida, A. Diez-Carlon, S. Y. Yang, Y.-M. Xie, X.-J. Gao, K. Watanabe, T. Taniguchi, X. Lu, K. T. Law, and D. K. Efetov, Magnetic Josephson Junctions and Superconducting Diodes in Magic Angle Twisted Bilayer Graphene, arXiv: 2110.01067 (2021).
- [17] E. Portolés, S. Iwakiri, G. Zheng, P. Rickhaus, T. Taniguchi, K. Watanabe, T. Ihn, K. Ensslin, and F. K. de Vries, A Tunable Monolithic SQUID in Twisted Bilayer Graphene, *Nat. Nanotechnol.* **17**, 1159 (2022).
- [18] B. Turini, S. Salimian, M. Carrega, A. Iorio, E. Strambini, F. Giazotto, V. Zannier, L. Sorba, and S. Heun, Josephson Diode Effect in High Mobility InSb Nanoflags, *Nano Lett.* **22**, 8502 (2022).
- [19] B. Pal, A. Chakraborty, P. K. Sivakumar, M. Davydova, A. K. Gopi, A. K. Pandeya, J. A. Krieger, Y. Zhang, M. Date, S. Ju, N. Yuan, N. B. M. Schröter, L. Fu, and S. S. P. Parkin, Josephson Diode Effect from Cooper Pair Momentum in a Topological Semimetal, *Nat. Phys.* **18**, 1228 (2022).
- [20] M. Gupta, G. V. Graziano, M. Pendharkar, J. T. Dong, C. P. Dempsey, C. Palmström, and V. S. Pribiag, Superconducting Diode Effect in a Three-Terminal Josephson Device, arXiv: 2206.08471 (2022).
- [21] C. Baumgartner, L. Fuchs, A. Costa, S. Reinhardt, S. Gronin, G. C. Gardner, T. Lindemann, M. J. Manfra, P. E. Faria Junior, D. Kochan, J. Fabian, N. Paradiso, and C. Strunk, Supercurrent Rectification and Magnetochiral Effects in Symmetric Josephson Junctions, *Nat. Nanotechnol.* **17**, 39 (2022).
- [22] C. Baumgartner, L. Fuchs, A. Costa, J. Picó-Cortés, S. Reinhardt, S. Gronin, G. C. Gardner, T. Lindemann, M. J. Manfra, P. E. Faria Junior, D. Kochan, J. Fabian, N. Paradiso, and C. Strunk, Effect of Rashba and Dresselhaus Spin-Orbit Coupling on Supercurrent Rectification and Magnetochiral Anisotropy of Ballistic Josephson Junctions, *J. Phys. Condens. Matter* **34**, 154005 (2022).
- [23] K.-R. Jeon, J.-K. Kim, J. Yoon, J.-C. Jeon, H. Han, A. Cottet, T. Kontos, and S. S. P. Parkin, Zero-Field Polarity-Reversible Josephson Supercurrent Diodes Enabled by a Proximity-Magnetized Pt Barrier, *Nat. Mater.* **21**, 1008 (2022).
- [24] H. Wu, Y. Wang, Y. Xu, P. K. Sivakumar, C. Pasco, U. Filippozzi, S. S. P. Parkin, Y.-J. Zeng, T. McQueen, and M. N. Ali, The Field-Free Josephson Diode in a van der Waals Heterostructure, *Nature* **604**, 653 (2022).
- [25] G. P. Mazur, N. van Loo, D. van Driel, J.-Y. Wang, G. Badawy, S. Gazibegovic, E. P. A. M. Bakkers, and L. P. Kouwenhoven, The Gate-Tunable Josephson Diode, arXiv: 2211.14283 (2022).
- [26] M. S. Anwar, T. Nakamura, R. Ishiguro, S. Arif, J. W. A. Robinson, S. Yonezawa, M. Sigrist, and Y. Maeno, Spontaneous Superconducting Diode Effect in Non-Magnetic Nb/Ru/Sr₂RuO₄ Topological Junctions, arXiv: 2211.14626 (2022).
- [27] T. Golod and V. M. Krasnov, Demonstration of a Superconducting Diode-with-Memory, Operational at Zero Magnetic Field with Switchable Nonreciprocity, *Nat. Commun.* **13**, 3658 (2022).
- [28] S. Ghosh, V. Patil, A. Basu, Kuldeep, D. A. Jangade, R. Kulkarni, A. Thamizhavel, and M. M. Deshmukh, High-Temperature Superconducting Diode, arXiv: 2210.11256 (2022).
- [29] J. Chiles, E. G. Arnault, C.-C. Chen, T. F. Q. Larson, L. Zhao, K. Watanabe, T. Taniguchi, F. Amet, and G. Finkelstein, Non-Reciprocal Supercurrents in a Field-Free Graphene Josephson Triode, arXiv: 2210.02644 (2022).
- [30] J. Hu, C. Wu, and X. Dai, Proposed Design of a Josephson Diode, *Phys. Rev. Lett.* **99**, 067004 (2007).
- [31] S. Hoshino, R. Wakatsuki, K. Hamamoto, and N. Nagaosa, Nonreciprocal Charge Transport in Two-Dimensional Noncentrosymmetric Superconductors, *Phys. Rev. B* **98**, 054510 (2018).
- [32] R. Wakatsuki and N. Nagaosa, Nonreciprocal Current in Noncentrosymmetric Rashba Superconductors, *Phys. Rev. Lett.* **121**, 026601 (2018).
- [33] B. Zhai, B. Li, Y. Wen, F. Wu, and J. He, Prediction of Ferroelectric Superconductors with Reversible Superconducting Diode Effect, *Phys. Rev. B* **106**, L140505 (2022).
- [34] J. J. He, Y. Tanaka, and N. Nagaosa, A Phenomenological Theory of Superconductor Diodes, *New J. Phys.* **24**, 053014 (2022).
- [35] H. D. Scammell, J. I. A. Li, and M. S. Scheurer, Theory of Zero-Field Superconducting Diode Effect in Twisted Trilayer Graphene, *2D Mater.* **9**, 025027 (2022).
- [36] S. Ilić and F. S. Bergeret, Theory of the Supercurrent Diode Effect in Rashba Superconductors with Arbitrary Disorder, *Phys. Rev. Lett.* **128**, 177001 (2022).
- [37] N. F. Q. Yuan and L. Fu, Supercurrent diode effect and finite-momentum superconductors, *Proc. Natl. Acad. Sci. USA* **119**, e2119548119 (2022).
- [38] A. Daido, Y. Ikeda, and Y. Yanase, Intrinsic Superconducting Diode Effect, *Phys. Rev. Lett.* **128**, 037001 (2022).
- [39] H. F. Legg, D. Loss, and J. Klinovaja, Superconducting Diode Effect Due to Magnetochiral Anisotropy in Topological Insulators and Rashba Nanowires, *Phys. Rev. B* **106**, 104501 (2022).
- [40] A. Daido and Y. Yanase, Superconducting Diode Effect and Nonreciprocal Transition Lines, arXiv: 2209.03515 (2022).
- [41] B. Zinkl, K. Hamamoto, and M. Sigrist, Symmetry Conditions for the Superconducting Diode Effect in Chiral Superconductors, *Phys. Rev. Res.* **4**, 033167 (2022).
- [42] C.-Z. Chen, J. J. He, M. N. Ali, G.-H. Lee, K. C. Fong, and K. T. Law, Asymmetric Josephson Effect in Inversion Symmetry Breaking Topological Materials, *Phys. Rev. B* **98**, 075430 (2018).
- [43] A. A. Kopasov, A. G. Kutlin, and A. S. Mel'nikov, Geometry Controlled Superconducting Diode and Anomalous Josephson Effect Triggered by the Topological Phase Transition in Curved Proximitized Nanowires, *Phys. Rev. B* **103**, 144520 (2021).
- [44] K. Misaki and N. Nagaosa, Theory of the Nonreciprocal Josephson Effect, *Phys. Rev. B* **103**, 245302 (2021).
- [45] K. Halterman, M. Alidoust, R. Smith, and S. Starr, Supercurrent Diode Effect, Spin Torques, and Robust Zero-Energy Peak in Planar Half-Metallic Trilayers, *Phys. Rev. B* **105**, 104508 (2022).
- [46] Y. Wei, H.-L. Liu, J. Wang, and J.-F. Liu, Supercurrent Rectification Effect in Graphene-Based Josephson Junctions, *Phys. Rev. B* **106**, 165419 (2022).
- [47] Y. Tanaka, B. Lu, and N. Nagaosa, Theory of Diode Effect in *d*-Wave Superconductor Junctions on the Surface

- of Topological Insulator, arXiv: 2205.13177 (2022).
- [48] Y. Zhang, Y. Gu, P. Li, J. Hu, and K. Jiang, General Theory of Josephson Diodes, *Phys. Rev. X* **12**, 041013 (2022).
 - [49] A. Soori, Nonequilibrium Josephson Diode Effect in Periodically Driven SNS Junctions, arXiv: 2206.07014 (2022).
 - [50] A. Soori, Anomalous Josephson Effect and Rectification in Junctions between Floquet Topological Superconductors, arXiv: 2208.08427 (2022).
 - [51] M. Davydova, S. Prembabu, and L. Fu, Universal Josephson Diode Effect, *Sci. Adv.* **8**, eabo0309 (2022).
 - [52] R. S. Souto, M. Leijnse, and C. Schrade, The Josephson Diode Effect in Supercurrent Interferometers, arXiv: 2205.04469 (2022).
 - [53] Y. V. Fominov and D. S. Mikhailov, Asymmetric Higher-Harmonic SQUID as a Josephson Diode, *Phys. Rev. B* **106**, 134514 (2022).
 - [54] B. Lu, S. Ikegaya, P. Burset, Y. Tanaka, and N. Nagaosa, Josephson Diode Effect on the Surface of Topological Insulators, arXiv: 2211.10572 (2022).
 - [55] Recent experiments in conventional superconductors [14] and high-temperature Josephson junction [28] reported recorded high diode efficiency of up to 60%. And the efficiency can reach 90% in another experiment on graphene-base Josephson triode [29]. But these cases are beyond our discussions because of the different mechanisms.
 - [56] L. Fu and C. L. Kane, Josephson current and noise at a superconductor/quantum-spin-Hall-insulator/superconductor junction, *Phys. Rev. B* **79**, 161408(R) (2009).
 - [57] C. W. J. J. Beenakker, D. I. Pikulin, T. Hyart, H. Schomerus, and J. P. Dahlhaus, Fermion-Parity Anomaly of the Critical Supercurrent in the Quantum Spin-Hall Effect, *Phys. Rev. Lett.* **110**, 017003 (2013).
 - [58] S.-P. Lee, K. Michaeli, J. Alicea, and A. Yacoby, Revealing Topological Superconductivity in Extended Quantum Spin Hall Josephson Junctions, *Phys. Rev. Lett.* **113**, 197001 (2014).
 - [59] S. Hart, H. Ren, T. Wagner, P. Leubner, M. Mühlbauer, C. Brüne, H. Buhmann, L. W. Molenkamp, and A. Yacoby, Induced superconductivity in the quantum spin Hall edge, *Nat. Phys.* **10**, 638 (2014).
 - [60] V. S. Pribiag, A. J. A. Beukman, F. Qu, M. C. Cassidy, C. Charpentier, W. Wegscheider, and L. P. Kouwenhoven, Edge-mode superconductivity in a two-dimensional topological insulator, *Nat. Nanotechnol.* **10**, 593 (2015).
 - [61] S. Hart, H. Ren, M. Kosowsky, G. Ben-Shach, P. Leubner, C. Brüne, H. Buhmann, L. W. Molenkamp, B. I. Halperin, and A. Yacoby, Controlled Finite Momentum Pairing and Spatially Varying Order Parameter in Proximitized HgTe Quantum Wells, *Nat. Phys.* **13**, 87 (2017).
 - [62] C. Huang, A. Narayan, E. Zhang, X. Xie, L. Ai, S. Liu, C. Yi, Y. Shi, S. Sanvito, and F. Xiu, Edge Superconductivity in Multilayer WTe₂ Josephson Junction, *Natl. Sci. Rev.* **7**, 1468 (2020).
 - [63] F. Lüpke, D. Waters, S. C. de la Barrera, M. Widom, D. G. Mandrus, J. Yan, R. M. Feenstra, and B. M. Hunt, Proximity-Induced Superconducting Gap in the Quantum Spin Hall Edge State of Monolayer WTe₂, *Nat. Phys.* **16**, 526 (2020).
 - [64] F. Dolcini, M. Houzet, and J. S. Meyer, Topological Josephson ϕ_0 junctions, *Phys. Rev. B* **92**, 035428 (2015).
 - [65] G. Tkachov, P. Burset, B. Trauzettel, and E. M. Hankiewicz, Quantum interference of edge supercurrents in a two-dimensional topological insulator, *Phys. Rev. B* **92**, 045408 (2015).
 - [66] B. Scharf, A. Braggio, E. Strambini, F. Giazotto, and E. M. Hankiewicz, Thermodynamics in Topological Josephson Junctions, *Phys. Rev. Res.* **3**, 033062 (2021).
 - [67] G. Blasi, F. Taddei, L. Arrachea, M. Carrega, and A. Braggio, Nonlocal Thermoelectricity in a Superconductor–Topological-Insulator–Superconductor Junction in Contact with a Normal-Metal Probe: Evidence for Helical Edge States, *Phys. Rev. Lett.* **124**, 227701 (2020).
 - [68] A. Zazunov, R. Egger, T. Jonckheere, and T. Martin, Anomalous Josephson Current through a Spin-Orbit Coupled Quantum Dot, *Phys. Rev. Lett.* **103**, 147004 (2009).
 - [69] J.-F. Liu and K. S. Chan, Anomalous Josephson current through a ferromagnetic trilayer junction, *Phys. Rev. B* **82**, 184533 (2010).
 - [70] J.-F. Liu and K. S. Chan, Relation between symmetry breaking and the anomalous Josephson effect, *Phys. Rev. B* **82**, 125305 (2010).
 - [71] T. Yokoyama, M. Eto, and Y. V. Nazarov, Josephson Current through Semiconductor Nanowire with Spin-Orbit Interaction in Magnetic Field, *J. Phys. Soc. Japan* **82**, 054703 (2013).
 - [72] T. Yokoyama, M. Eto, and Y. V. Nazarov, Anomalous Josephson Effect Induced by Spin-Orbit Interaction and Zeeman Effect in Semiconductor Nanowires, *Phys. Rev. B* **89**, 195407 (2014).
 - [73] N. F. Q. Yuan and L. Fu, Zeeman-Induced Gapless Superconductivity with a Partial Fermi Surface, *Phys. Rev. B* **97**, 115139 (2018).
 - [74] N. F. Q. Yuan and L. Fu, Topological Metals and Finite-Momentum Superconductors, *Proc. Natl. Acad. Sci.* **118** (3) e2019063118 (2021).
 - [75] M. Ezawa, Photoinduced Topological Phase Transition and a Single Dirac-Cone State in Silicene, *Phys. Rev. Lett.* **110**, 026603 (2013).
 - [76] M. N. Chen, W. Su, M. X. Deng, J. Ruan, W. Luo, D. X. Shao, L. Sheng, and D. Y. Xing, Photoinduced Topological Phase Transition and Spin Polarization in a Two-Dimensional Topological Insulator, *Phys. Rev. B* **94**, 205429 (2016).
 - [77] S. S. Dabiri, H. Cheraghchi, and A. Sadeghi, Light-Induced Topological Phases in Thin Films of Magnetically Doped Topological Insulators, *Phys. Rev. B* **103**, 205130 (2021).
 - [78] P.-H. Fu, Y. Xu, X.-L. Yu, J.-F. Liu, and J. Wu, Electrically Modulated Josephson Junction of Light-Dressed Topological Insulators, *Phys. Rev. B* **105**, 064503 (2022).
 - [79] C.-Z. Chen, J. Qi, D.-H. Xu, and X. Xie, Evolution of Berry Curvature and Reentrant Quantum Anomalous Hall Effect in an Intrinsic Magnetic Topological Insulator, *Sci. China Physics, Mech. Astron.* **64**, 127211 (2021).
 - [80] D. Zhang, M. Shi, T. Zhu, D. Xing, H. Zhang, and J. Wang, Topological Axion States in the Magnetic Insulator MnBi₂Te₄ with the Quantized Magnetoelectric Effect, *Phys. Rev. Lett.* **122**, 206401 (2019).
 - [81] D. S. Holmes, Cryogenic Electronics and Quantum Information Processing, in 2021 IEEE International Roadmap for Devices and Systems Outbriefs (IEEE, 2021), pp. 1–93.

- [82] See Supplemental Material at [URL will be inserted by publisher] for (i) the Doppler energy shift in AHESs, (ii) the analytical method to obtain Andreev bound states, the current-phase relations, and the diode efficiency in a short Josephson junction, and (iii) the numerical calculations using a tight-binding model with arbitrary junction length.
- [83] C. W. J. Beenakker, Universal limit of critical-current fluctuations in mesoscopic Josephson junctions. *Phys. Rev. Lett.* **67**, 3836–3839 (1991).
- [84] C. Beenakker, Three “universal” mesoscopic Josephson effects, in *Transport Phenomena in Mesoscopic Systems* Eds. Hidetoshi Fukuyama, Tsuneya Ando (Springer, 1992) pp. 235–253.
- [85] G. Tkachov, Soliton Defects and Topological-Periodic Superconductivity from an Orbital Magnetic Field Effect in Edge Josephson Junctions, *J. Phys. Condens. Matter* **31**, 175301 (2019).
- [86] G. Tkachov, Chiral Current-Phase Relation of Topological Josephson Junctions: A Signature of the 4π -Periodic Josephson Effect, *Phys. Rev. B* **100**, 035403 (2019).
- [87] B. A. Bernevig, T. L. Hughes, and S.-C. Zhang, Quantum Spin Hall Effect and Topological Phase Transition in HgTe Quantum Wells, *Science* **314**, 1757 (2006).
- [88] C.-X. Liu, X.-L. Qi, X. Dai, Z. Fang, and S.-C. Zhang, Quantum Anomalous Hall Effect in $\text{Hg}_{1-y}\text{Mn}_y\text{Te}$ Quantum Wells, *Phys. Rev. Lett.* **101**, 146802 (2008).
- [89] J. Zou and G. Jin, Exchange-Field-Modulated $0-\pi$ Transition and Chiral Edge Supercurrents in a Superconductor/Ferromagnetic Topological Insulator/Superconductor Junction, *Phys. Rev. B* **85**, 134528 (2012).
- [90] Y. Xu, S. Uddin, J. Wang, Z. Ma, and J.-F. Liu, Electrically Modulated SQUID with a Single Josephson Junction Coupled by a Time Reversal Breaking Weyl Semimetal Thin Film, *Phys. Rev. B* **97**, 035427 (2018).
- [91] P.-H. Fu, J. Wang, J.-F. Liu, and R.-Q. Wang, Josephson Signatures of Weyl Node Creation and Annihilation in Irradiated Dirac Semimetals, *Phys. Rev. B* **100**, 115414 (2019).
- [92] J. Chen, W. Xu, Z. Tan, Z. Pan, P. Zhu, Z.-M. Liao, and D. Yu, Superconducting Proximity in Intrinsic Magnetic Topological Insulator MnBi_2Te_4 -NbN Hybrid Device Modulated by Coulomb Blockade Effect, *Nano Lett.* **22**, 6484 (2022).
- [93] W.-Z. Xu, C.-G. Chu, Z.-C. Pan, J.-J. Chen, A.-Q. Wang, Z.-B. Tan, P.-F. Zhu, X.-G. Ye, D.-P. Yu, and Z.-M. Liao, Proximity-Induced Superconducting Gap in the Intrinsic Magnetic Topological Insulator MnBi_2Te_4 , *Phys. Rev. B* **105**, 184515 (2022).
- [94] G. De Simoni, F. Paolucci, C. Puglia, and F. Giazotto, Josephson Field-Effect Transistors Based on All-Metallic Al/Cu/Al Proximity Nanojunctions, *ACS Nano* **13**, 7871 (2019).
- [95] Z. Xu, W. Chen, J. Huang, W. Tian, S. Chen, W. Yue, T. Chi, Y.-Y. Lyu, H. Sun, Y.-L. Wang, G. Sun, J. Chen, B. Jin, S.-L. Li, H. Yuan, J. Li, D. Koelle, R. Kleiner, H. Wang, and P. Wu, Vertical Josephson Field-Effect Transistors Based on Black Phosphorus, *Appl. Phys. Lett.* **119**, 072601 (2021).